JOURNAL OF SOLID STATE CHEMISTRY 107, 264–272 (1993)

Phase Diagram, Lattice Parameter, and Optical Energy Gap Values for the $Cd_{2x}(CuGa)_yMn_{2z}Te_2$ Alloys

R. GOUDREAULT AND J. C. WOOLLEY

Ottawa–Carleton Institute for Physics, University of Ottawa, Ottawa, Ontario K1N 6N5, Canada

AND M. QUINTERO AND R. TOVAR

Departamento de Física, Universidad de Los Andes, Mérida, Venezuela

Received December 7, 1992; in revised form March 17, 1993; accepted March 22, 1993

The T vs composition phase diagram of the alloy system $Cd_{2x}(CuGa)_yMn_{2z}Te_2$ ($x + y + z = 1$) was investigated in the range $0 < z < 0.8$ by differential thermal analysis and X-ray diffraction measurements. Samples were prepared for various lines of constant x/y ratio and the $T(z)$ data were determined for each line. X-ray powder photographs were used to determine equilibrium conditions, to give lattice parameter values, and to determine the limits of single-phase solid solution. In addition to the various phase field boundaries, the zinc-blend–chalcopyrite and Mn-ordered–Mn-disordered transition lines were determined, these fields being the ones of interest in the measurements of optical energy gap and magnetic properties. Room-temperature values of the optical energy gap E_0 were determined for all of the single-phase samples and the variations of E_0 with z were investigated.

Introduction

Most of the work on semimagnetic semiconductor alloys (*1*) has been concerned with alloys of the form $II_{1-z}Mn_zVI$. However, similar alloys can be produced from the chalcopyrite $I.III.VI_2$ compounds, the ternary analogues of the II.VI compounds. A number of alloy systems of the form $(I.III)_{1-z}Mn_{2z}Te_2$ have been investigated and this work has been extended to the more general $II_{2x}(I.III)_yMn_{2z}Te_2$ alloys (*2–8*). It has been shown that in almost all cases the solid solubility of the MnTe in the zinc-blend/chalcopyrite phase extends over a wide range of z values. Alloys in this single-phase range are of interest because, depending upon the heat treatment, the alloys can be produced either with the Mn atoms at random on the cation sublattice or with the Mn atoms ordered. The optical energy gap values and the magnetic behavior are very different under the two different conditions (*2, 3, 6, 9, 10*). Before a detailed investigation of effects of Mn ordering can be carried out, a knowledge of the phase diagram of the alloy system is required. For the case of the Cd alloys, these data have been obtained for the cases of $Cd_{2x}(CuIn)_yMn_{2z}Te_2$ (*11*) and $Cd_{2x}(AgIn)_yMn_{2z}Te_2$ (*12*) systems. Work on the $(CuGa)_{1-z}Mn_{2z}Te_2$ system (*13*) has shown that its behavior is quite different from those of the corresponding CuIn (*11*), AgIn (*12*), and AgGa (*6*) alloys, in that the range of solid solubility of Mn in $CuGaTe_2$ is very small. Earlier investigations of the $Cd_{2x}(CuGa)_{1-x}Te_2$ system (*14*) showed that solid solubility in the zinc-blend CdTe phase extends from $x = 1$ to $x = 0.33$, but that for x smaller than this, there appears to be two-phase behavior except for alloys very close to $CuGaTe_2$. In

0022-4596/93 $5.00

the present work, the system $Cd_{2x}(CuGa)_y Mn_{2z}Te_2$ has been investigated, so as to obtain information on the range of zinc-blend/chalcopyrite solid solubility in this case, and to determine phase diagram, lattice parameter, and optical energy gap values.

Preparation of Samples and Experimental Measurements

In order to facilitate comparison of results, samples were made at compositions along lines of constant $x:y$ ratio, i.e., $x = 3y$, $x = y$, $3x = y$, $7x = y$, and $x = 0$, at various fixed values of z, and also a few samples along the line $y = 0.5$. As in previous cases, since the interest of the research programme is in semimagnetic semiconductor alloys, the Mn-rich phases were not investigated.

All of the alloys were produced by the usual melt-and-anneal technique (*15*). The components of each 1-g sample were sealed under vacuum in a small quartz ampoule, the inside surface of which had previously been carbonized to prevent interaction of the alloy with the quartz, were heated to 1150°C and allowed to react. Each sample was then slowly cooled in the furnace to room temperature and then was annealed to equilibrium at an appropriate temperature. Except where indicated differently below, the annealing temperature was 600°C, and after annealing the sample was slowly cooled to room temperature over approximately 10 hr.

For each sample so produced, room-temperature X-ray Debye–Scherrer photographs were made on powdered specimens to check the equilibrium conditions and to determine whether a single phase form was present. Values of lattice parameters were determined for all cases where chalcopyrite or zinc-blend phase were present, germanium being used as an internal standard where required.

Transition temperatures were obtained from differential thermal analysis (DTA) measurements (*16*), with silver being used as the reference material. The charge used was in powdered form and was approximately 100 mg weight. This was sealed under vacuum in a small quartz ampoule which had a re-entrant thermocouple well at the bottom. The temperatures of the sample and the reference were measured with chromel–alumel thermocouples, the difference signal between the sample and the reference and the temperature signal being registered on a chart recorder. Each phase transition temperature was determined from the base line intercept of the tangent to the leading edge of the peak in the difference signal. Both heating and cooling runs were made for each sample.

Slices of each single-phase sample were cut and thinned down to give specimens for standard optical absorption work (*17*). Values of $(1/d)\ln(I_0/I)$, where d is the thickness (of approximately 100μm), I_0 the incident intensity, and I the transmitted intensity, were determined as a function of photon energy $h\nu$ and corrected by subtracting a background value to give the absorption coefficient α. The relation $\alpha h\nu = A(E_0 - h\nu)^{1/2}$ was then used to give a value for E_0, by plotting graphs of $(\alpha h\nu)^2$ versus $h\nu$ and taking the intercept on the $h\nu$ axis as E_0.

Phase Diagram Results

For these alloys, DTA results for the $y = 0$ ($Cd_{1-z}Mn_zTe$) and the $x = 0$ ($(CuGa)_{1-z}Mn_{2z}Te_2$) lines were published previously (*18, 13*). In the case of $z = 0$, X-ray analysis showed that single-phase solid solution occurred in the composition ranges $1.0 > x > 0.33$ and $\sim 0.02 > x > 0$ (*14*), but the phase conditions at higher temperatures were not determined. Hence this range has been treated in some detail here. For the $x = 0$ line, the T–z phase diagram was published (*13*), but a few changes have been made in the light of the present results. Detailed DTA and X-ray diffraction measurements were carried out on the $y = 3x$, $y = x$, and $x = 3y$ sections, and X-ray measurements on the $y = 7x$ section.

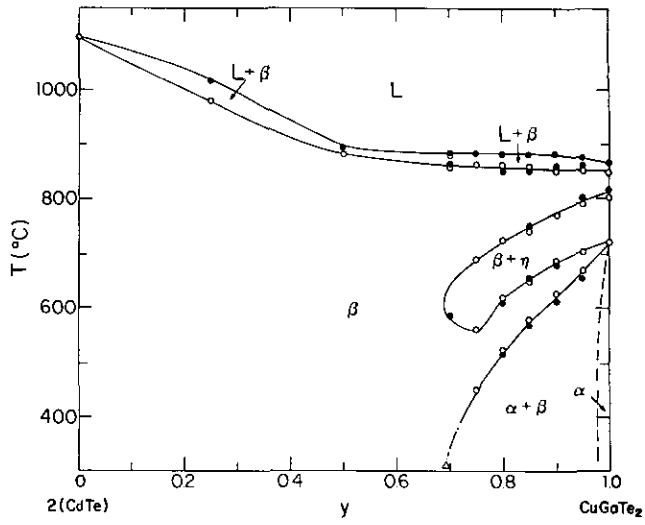

Fig. 1. $T(y)$ diagram for $z = 0$ section ($Cd_{2x}(CuGa)_{1-x}Te_2$): (○) DTA heating run, (●) DTA cooling run, and (△) from X-ray data.

The DTA data for the various sections are shown in Figs. 1–5 and the lattice parameter values in Figs. 6–8. For the $z = 0$ section, Figs. 1 and 6 show that at 300°C and below, the range of solid solubility is in good agreement with previous work, with zinc-blend β solid solution extending from $y = 0$ to $y = \sim 0.68$ and chalcopyrite α from $y = 1.0$ to $y = \sim 0.97$. In the intermediate composition range, the behavior is more complicated. At the lower temperatures, there is a two-phase field, $(\alpha + \beta)$, with tie-lines lying in the plane of the diagram, and above that a narrow single phase β field, extending from $T = 450$–560°C at $y = 0.75$ to $T = 740$°C at $y = 1.0$. Above this again, there is a two-phase $(\beta + \eta)$ field in which both of the equilibrium phases lie outside the section being considered here, and occur on the Ga_2Te_3–Cu_2Te section as shown in Fig. 9. Finally, in a temperature range around 850°C, single-phase zinc-blend β occurs across the complete composition range. From Fig. 6, it is seen that the lattice parameter a varies linearly with y across the zinc-blend β field.

For the $x = 0$ section, the revised T–z diagram and the lattice parameter variation are shown in Figs. 2 and 7. In the T–z diagram, the form below 600°C is unchanged (*13*), but above 600°C the shapes of some of the fields have been altered, particularly the β and $(\beta + \eta)$ fields to be more consistent

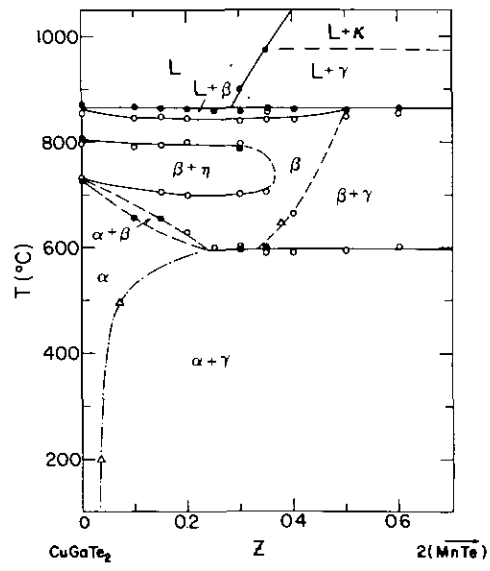

FIG. 2. $T(z)$ diagram for $x = 0$ section ($(CuGa)_{1-z}Mn_{2z}Te_2$): (○) DTA heating run, (●) DTA cooling run, and (△) X-ray data.

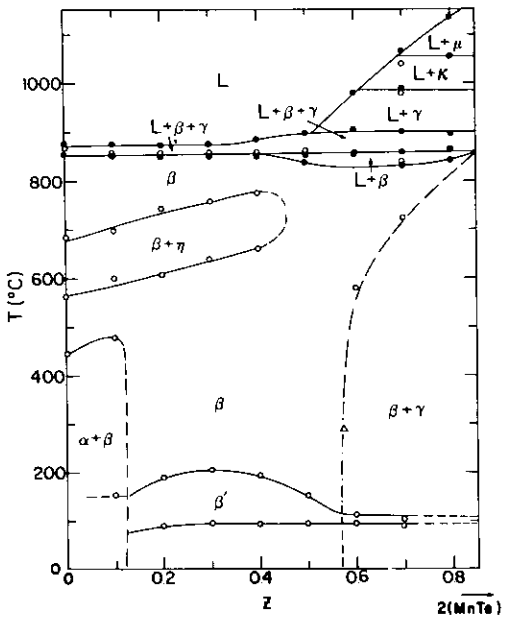

FIG. 3. $T(z)$ diagram for $y = 3x$ section: (○) DTA heating run, (●) DTA cooling run, and (△) from X-ray data.

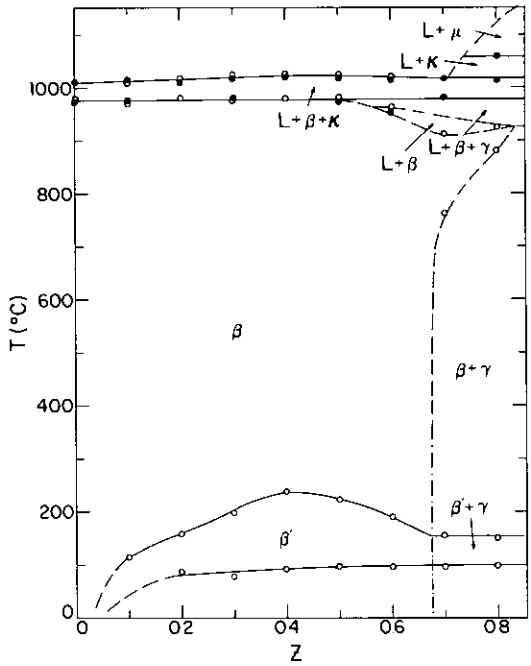

FIG. 5. $T(z)$ diagram for $x = 3y$ section: (○) DTA heating run, (●) DTA cooling run, and (△) from X-ray data.

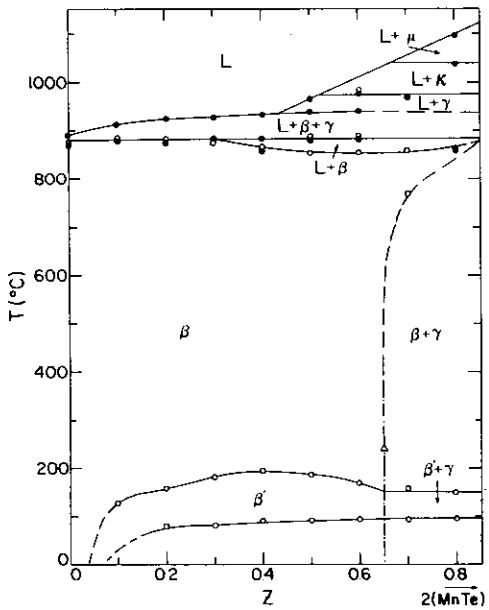

FIG. 4. $T(z)$ diagram for $x = y$ section: (○) DTA heating run, (●) DTA cooling run, and (△) from X-ray data.

with the form of the $z = 0$ section. In Fig. 7, the variation of the lattice parameter a with z is very similar to that shown previously (*13*).

The T–z data for the sections $y = 3x$, $y = x$, and $x = 3y$ are shown in Figs. 3, 4, and 5 and the lattice parameter data for those sections plus $y = 7x$ in Fig. 8. From the

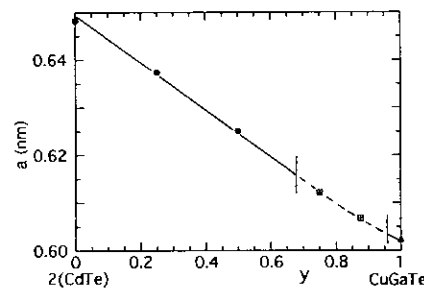

FIG. 6. Variation of lattice parameter a with x for the $z = 0$ section ($Cd_{2x}(CuGa)_{1-x}Te_2$): (●) measured zinc-blend values, (▲) measured chalcopyrite value, (⊞) values from extrapolation to $z = 0$ of a vs z lines (see Fig. 8).

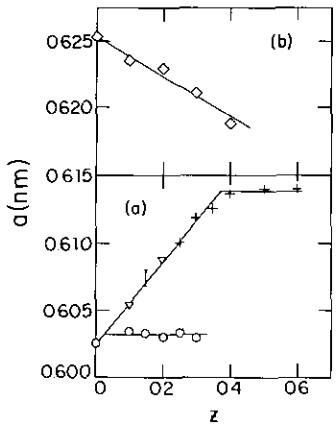

FIG. 7. Variation of lattice parameter a with z for (a) the $x = 0$ section ($(CuGa)_{1-z}Mn_{2z}Te_2$) and (b) the $y = 0.5$ section. In (a): (○) chalcopyrite annealed at 200°C: (I) and (△) chalcopyrite quenched from 650°C, (+) zinc-blend quenched from 650°C.

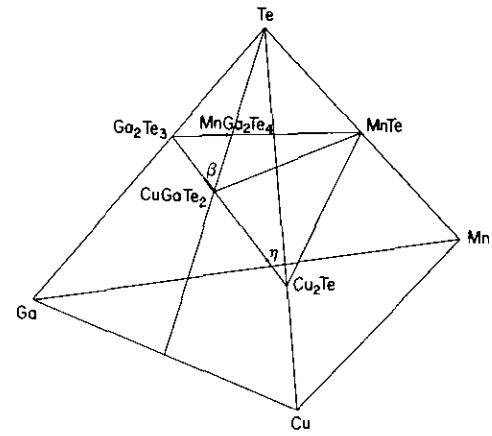

FIG. 9. Composition diagram of Cu–Ga–Mn–Te system, showing Cu_2Te–Ga_2Te_3–MnTe plane and $CuGaTe_2$–MnTe line.

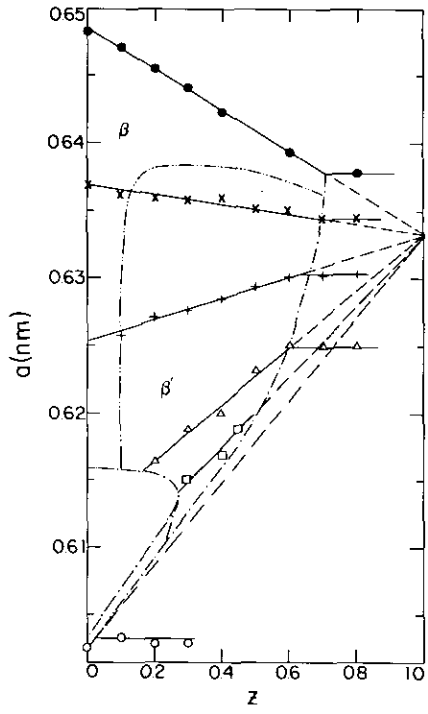

FIG. 8. Variation of lattice parameter a with z for various sections: (●) $y = 0$, (x)$x = 3y$; (+) $x = y$; (△) $y = 3x$; (□) $y = 7x$; (○) $x = 0$; (_._._) phase boundary; (_.._.._) order–disorder boundary.

X-ray data in Fig. 8, it is seen that there is no single phase α in any of these sections, although two-phase ($\alpha + \beta$) fields occur in the $y = 7x$ and $y = 3x$ sections corresponding to that in the $z = 0$ section. In all cases, there is a wide range of solubility in the zinc-blend β phase, the limit extending from $z = 0.50$ in the $y = 7x$ section to $z = 0.70$ for $x = 3y$. These values have been taken to be the positions of the β–($\beta + \gamma$) phase boundaries at ~300°C in the various sections as seen in Figs. 3, 4, and 5. In all cases, the variation of the zinc-blend lattice parameter a with z is seen to be linear, and these lines all extrapolate to a value of $a = 0.6333$ nm at $z = 0$, in good agreement with the value obtained in other similar alloy systems (*2, 3, 7, 8*). In the $y = 7x$ and $y = 3x$ cases, the single-phase β field does not extend to $z = 0$, but extrapolation of the straight lines gives values of a corresponding to $z = 0$ and, as seen in Fig. 6, these fit well with the experimental values determined for the other lines.

With regard to the $T(z)$ diagrams for the $y = 3x$, $y = x$, and $x = 3y$ sections, the $y = 3x$ section shows, as indicated above, the two-phase ($\alpha + \beta$) field at low z and temperatures below 480°C and also, at higher temperatures, a two-phase ($\beta + \eta$) field corre-

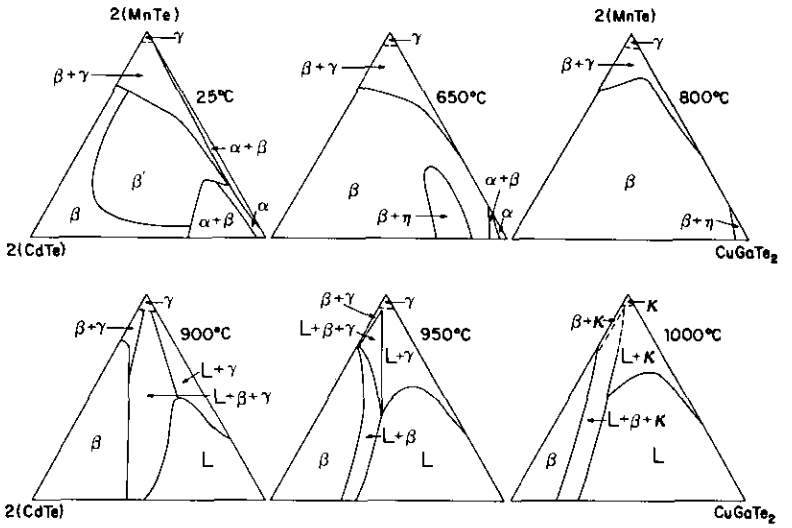

FIG. 10. Isothermal sections of the $Cd_{2x}(CuGa)_yMn_{2z}Te_2$ at the temperatures indicated.

sponding to those occurring in the $z = 0$ and $x = 0$ sections (Figs. 1 and 2). Except for these two two-phase fields, the three sections show, in general, very similar form one to another. In each case, the β field extends to a z value in the range 0.6–0.7, and at higher z values a two-phase ($\beta + \gamma$) field occurs, γ being the NiAs structure of MnTe. Also in each section, in the vicinity of 200°C, the zinc-blend-type phase changes from a Mn-disordered β structure to the Mn-ordered β' form, reported previously for a number of alloy systems of this type (*5, 6, 8, 10*). It has been suggested (*4, 5*) that this ordered structure is based on the stannite form, but the detail of the structure has not, as yet, been completely determined. At about 100°C, a second ordering transition occurs but no information on the lower field has yet been obtained. In all three sections, the β field is lost somewhere in the temperature range 800–1000°C, to be replaced by two- and three-phase fields of the form ($L + \beta$), ($L + \beta + \gamma$), etc. The diagrams are complicated in this range by the different structures which are shown by MnTe, and which have been labelled progressively with temperature as γ, κ, and μ in Figs. 3, 4, and 5. For these higher temperature fields, it is clear from a consideration of possible tie-lines that any β phase which occurs must have a composition lying outside the composition triangle CdTe–$CuGaTe_2$–MnTe. In the cases of the similar $Hg_{2x}(AgIn)_yMn_{2z}Te_2$ and $Hg_{2x}(CuIn)_yMn_{2z}Te_2$ alloys (*8*), it was indicated that the β field in those cases extended from the β solid solution between $AgInTe_2$ ($CuInTe_2$) and In_2Te_3 to $MnIn_2Te_4$. Figure 9 shows the corresponding phases, $CuGaTe_2$ solid solution and $MnGa_2Te_4$, in the present case. The structure of $MnGa_2Te_4$ does not seem to have been investigated, but it is quite possible that a similar β field exists in this system and that the high temperature β phases in the present diagram are related to it. From the five vertical sections shown in Figs. I–5, plus that for the CdTe–MnTe section (*18*), it is possible to give reasonable estimates of various isothermal sections of the phase diagram. Such isothermal sections for the temperatures 25, 650, 800, 900, 950, and 1000°C are shown in Fig. 10.

Optical Results

Experimental values of the optical energy gap E_0 are shown for the sections $x = 0$ and

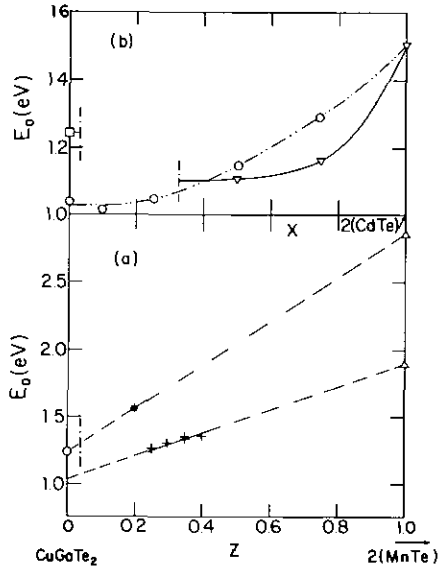

FIG. 11. (a) Variation of the optical energy gap E_0 with z for the $x = 0$ section: (+) zinc-blend quenched from 650°C, (*) chalcopyrite quenched from 650°C, (○) chalcopyrite slowly cooled to room temperature, and (△) extrapolated values at $z = 1.0$. (b) Variation of E_0 with x for the $z = 0$ section: (△) zinc-blend slowly cooled to room temperature, (□) chalcopyrite slowly cooled to room temperature, (○) and (_.._.._) extrapolated to $z = 0$ from ordered cubic range (see Fig. 12), and (_._._) single-phase limit at room temperature.

$z = 0$ in Figs. 11a and 11b and for the other sections investigated in Fig. 12. In Fig. 11b, it is seen that in the zinc-blend range of the $z = 0$ section ($Cd_{2x}(CuGa)_{1-x}Te_2$), the value of E_0 falls rapidly from the value of 1.50 eV for CdTe with addition of relatively small amounts of $CuGaTe_2$, but for $x < \sim 0.75$ levels out and becomes almost constant. Similar behaviour has been observed previously (*2, 7, 14, 19, 20*) for corresponding alloy systems, e.g., $Cd_{2x}(CuIn)_{1-x}Te_2$, $Cd_{2x}(CuIn)_{1-x}Se_2$, $Zn_{2x}(AgIn)_{1-x}Te_2$, etc. Extrapolation of this E_0 vs x line indicates a value of ~1.1 eV at $x = 0$, i.e., for $CuGaTe_2$ in the zinc-blend form. This will be discussed further below. The measured value for E_0 for chalcopyrite $CuGaTe_2$ is shown in Fig. 11b as 1.24 eV.

Values of E_0 for the $x = 0$ ($(CuGa)_{1-z}Mn_{2z}Te_2$) were published previously (*13*) and are reproduced in Fig. 11a for comparison purposes. Samples with $z > 0.2$ and quenched from 650°C were found to be single-phase zinc-blend and gave energy gap values as shown. However, the sample with $z = 0.2$ and quenched from 650°C had chalcopyrite structure and gave an appreciably higher value of E_0. The variations of E_0 with z for the other four sections involving $CuGaTe_2$ are shown in Fig. 12. It is seen that in all cases except for one point at $z = 0.1$ on the $x = 3y$ section, the values obtained in each section give a linear variation of E_0 with z, and in all cases these lines extrapolate to $E_0 = 1.86$ eV at $z = 1$. As shown previously (*2, 3, 6, 7*), the values of E_0 obtained by extrapolation to $z = 1$ are characteristic of the structure of the samples considered. Thus the Mn-disordered zinc-blend β phase gives a value of 2.85 eV, the Mn-ordered zinc-blend β' phase 1.85 eV, and the Mn-ordered chalcopyrite α' phase 1.35 eV, while the value for the Mn-disordered chalcopyrite α phase has not been accurately determined but appears to be in the range 2.6–2.85 eV. Thus the present samples must be in the β' form. When considered in conjunction with the $z = 0$ point on the same section, the differing point at $z = 0.1$ on the $x = 3y$ line appears to be in the α condition, the line joining the two points extrapolating to $E_0 = \sim 2.8$ eV at $z = 1$, as

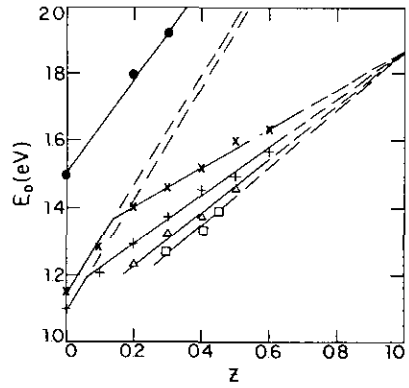

FIG. 12. Variation of optical energy gap E_0 with z for various sections; (●) $y = 0$; (×) $x = 3y$, (+) $x = y$, (△) $y = 3x$, and (□) $y = 7x$.

indicated in Fig. 12. The intersection of this line with that for the Mn-ordered zinc-blend β' phase gives the boundary between the β & β' fields and this is shown in Fig. 8 for the $x = 3y$ and $x = y$ lines.

If the straight lines of E_o vs z in the β' field are extrapolated to $z = 0$, again values of E_o corresponding to a zinc-blend form with $z = 0$ are obtained, and these are shown in Fig. 11b. It is seen that these are appreciably different from those measured for the $z = 0$ alloys. Thus an attempt to find a value of E_o for $CuGaTe_2$ in zinc-blend form will give different values depending upon which extrapolation is used, e.g., the two values of 1.10 and 1.03 eV obtained in the present case. Taking a mean of 1.06 eV from these two values with the experimental value of E_o for chalcopyrite $CuGaTe_2$ of 1.24 eV, the difference between the chalcopyrite and zinc-blend values is about 0.18 eV. Similar estimates of this difference have been made previously (*5, 6, 7, 9, 13*) for several other I.III.VI_2 compounds and values of the order 0.25 eV obtained. Various theoretical studies have been made to estimate the value of this difference. Thus Zunger (*21*) indicated a value of 0.4 eV, while Rincon (*22*) predicted values lying in the range 0.42–0.50 eV. The present experimental values are appreciably smaller than these theoretical ones.

Conclusions

The results show that although the range of solid solution in the chalcopyrite phase is very limited, there is a wide range of solid solution in the zinc-blend phase. In all sections investigated, the ordering transition β–β' involving the Mn atoms was observed at about 200°C. At higher temperatures, the diagram in the vicinity of $CuGaTe_2$ is complicated by the occurrence of a two-phase field, $(\beta + \eta)$, where both phases lie outside the triangular section being investigated here. Also, at higher temperatures three phase fields occur, which probably involve a phase of composition close to $MnGa_2Te_4$. The Mn-ordering behavior, previously described for various similar I–III chalcopyrite systems, was observed at values of z greater than ~0.1, but with transition temperatures at only 200°C or less.

The values of the optical energy gap E_o showed similar behavior to those for associated chalcopyrite alloy systems, with E_o varying linearly with z in the various sections of constant c/a, and extrapolating to a value of 1.86 eV at $z = 1.0$, typical of the Mn-ordered zinc-blend β' alloys, as shown previously for other similar alloy systems.

Acknowledgments

The Venezuelan authors are grateful to Consejo Nacional de Investigaciones Científicas y Tecnológicas (CONICIT) and Consejo de Desarollo Científico, Humanístico y Tecnológico (CDCHT-ULA) for financial support.

References

1. J. K. Furdyna and J. Kossut, *in* "Diluted Magnetic Semiconductors" (Willardson and Beer, Eds.), Semimetals and Semiconductors, Vol. 25, Academic Press, San Diego (1989).
2. M. Quintero, L. Dierker, and J. C. Woolley, *J. Solid State Chem.* **63,** 110 (1986).
3. M. Quintero and J. C. Woolley, *Phys. Status Solidi A* **92,** 449 (1985).
4. A. Aresti, L. Garbato, A. Geddo-Lehmann, and P. Manca, *in* "Proceedings, 7th International Conference on Ternary and Multinary Compounds," p. 497, Materials Research Soc., Pittsburgh (1986).
5. M. Quintero, P. Grima, R. Tovar, G. S. Perez, and J. C. Woolley, *Phys. Status Solidi A* **107,** 205 (1988).
6. M. Quintero, R. Tovar, M. Al-Najjar, G. Lamarche, and J. C. Woolley, *J. Solid State Chem.* **74,** 136 (1988).
7. C. Neal, J. C. Woolley, R. Tovar, and M. Quintero, *J. Phys. D: Appl. Phys.* **22,** 1347 (1989).
8. P. Grima, M. Quintero, and J. C. Woolley, *J. Cryst. Growth* **119,** 381 (1992).
9. M. Quintero, P. Grima, J. E. Avon, G. Lamarche and J. C. Woolley, *Phys. Status Solidi A* **108,** 794 (1988).
10. G. Lamarche, J. C. Woolley, R. Tovar, M. Quintero and V. Sagredo, *J. Magn. Magn. Mater.* **80,** 321 (1989).
11. M. Quintero, E. Guerrero, R. Tovar, S. Perez

AND J. C. WOOLLEY, *J. Solid State Chem.* **87,** 456 (1990).
12. M. QUINTERO, E. GUERRERO, P. GRIMA, AND J. C. WOOLLEY, *J. Electrochem. Soc.* **136,** 1220 (1989).
13. M. QUINTERO, P. GRIMA, R. TOVAR, R. GOUDREAULT, D. BISSONNETTE, G. LAMARCHE, AND J. C. WOOLLEY, *J. Solid State Chem.* **76,** 210 (1988).
14. J. C. WOOLLEY AND E. W. WILLIAMS, *J. Electrochem. Soc.* **113,** 899 (1966).
15. R. BRUN DEL RE, T. DONOFRIO, J. E. AVON, J. MAJID, AND J. C. WOOLLEY, *Nuovo Cimento Soc. Ital. Fiz. D* **2,** 1911 (1983).
16. R. CHEN AND Y. KIRSH, "Analysis of Thermally Stimulated Processes, Intern. Series on Science of the Solid State," Vol. 15, p. 97, Pergamon, Oxford (1981).
17. R. G. GOODCHILD, O. H. HUGHES, S. A. LOPEZ-RIVERA, AND J. C. WOOLLEY, *Can. J. Phys.* **60,** 1096 (1982).
18. R. TRIBOULET AND G. DIDIER, *J. Cryst. Growth* **52,** 614 (1981).
19. L. GARBATO, F. LEDDA, P. MANCA, A. RUCCI, AND A. SPIGA, *Prog. Cryst. Growth Charact.* **10,** 199 (1985).
20. L. GARBATO, F. LEDDA, AND P. MANCA, *Jpn. J. Appl. Phys.* **19,** 67 (1980).
21. A. ZUNGER, *Appl. Phys. Lett.* **50,** 164 (1987).
22. C. RINCON, *Solid State Commun.* **64,** 663 (1987).